This is the author version of an article published in:
J.M. Borrajo, S. Zucca, M.M. Gola, Analytical formulation of the Jacobian matrix for non-linear calculation of the forced response of turbine blade assemblies with wedge friction dampers, International Journal of Non-Linear Mechanics, Volume 41, Issue 10, December 2006, Pages 1118-1127, ISSN 0020-7462, 10.1016/j.ijnonlinmec.2006.11.003.
The article is available on-line at:
http://www.sciencedirect.com/science/article/pii/S0020746206001016

Analytical Formulation of the Jacobian Matrix for Non-linear Calculation of the Forced Response of Turbine Blade Assemblies with Wedge Friction Dampers.

Borrajo, J.M.; Zucca*, S.; Gola, M.M.
Department of Mechanical Engineering – Politecnico di Torino
Corso Duca degli Abruzzi 24, 10129 Torino – ITALY

Abstract

A fundamental issue in turbomachinery design is the dynamical stress assessment of turbine blades. In order to reduce stress peaks in the turbine blades at engine orders corresponding to blade natural frequencies, friction dampers are employed. Blade response calculation requires the solution of a set of nonlinear equations originated by the introduction of friction damping.

Such a set of nonlinear equations is solved using the iterative numerical Newton-Raphson method. However, calculation of the Jacobian matrix of the system using classical numerical finite difference schemes makes frequency domain solver prohibitively expensive for structures with many contact points. Large computation time results from the evaluation of partial derivatives of the nonlinear equations with respect to the displacements.

In this work a methodology to compute efficiently the Jacobian matrix of a dynamic system having wedge dampers is presented. It is exact and completely analytical.

The proposed methods have been successfully applied to a real intermediate pressure turbine (IPT) blade under cyclic symmetry boundary conditions with underplatform wedge dampers. Its implementation showed to be very effective, and allowed to achieve relevant time savings without loss of precision.

* Corresponding author – tel. +39 011 5646933 – email: stefano.zucca@polito.it

Keywords

Non-linear dynamics, forced response, turbine blades, wedge dampers, friction damping.

1. Introduction

Service failure of turbo-engine blades in many instances can be attributed to high cyclic fatigue, HCF, caused by large resonant stress. Blades are subjected to forced vibrations caused by variation of the flow of air drawn through compressor and turbine stages in space and time, blade hub, meshing of gear teeth, foreign object ingestion, etc.

Commonly the frequency spectrum of the external periodic forces has components which excite dominant cantilevered-blade modes of the system causing resonances, manifesting in a sharp increase of response amplitude.

Nowadays, in order to avoid such failures, designers frequently include friction dampers to increase blade damping and reduce vibratory stresses. The introduction of friction dampers originates the nonlinearities in the system that turns the prediction of its dynamic response very difficult.

Friction damping has been largely studied in the literature. It has long been recognized to be an effective and simple mean of increasing the mechanical damping level of turbine bladed disk systems [1-3]. Application of friction damping for blade vibration control was first studied for blade-to-ground and blade-to-blade (shroud) configurations [4,5]. Whatever configuration is chosen, damper kinematic model plays an important role in friction force calculation, since friction is due to relative displacements of mating surfaces.

Currently, a widespread damper type is the so called underplatform wedge damper, it is a simple metallic piece located at the blade roots. In an operating engine, centrifugal force acting on the damper lifts it gradually and, at a certain speed, it fully engages the platform at the ad-hoc designed cavity. Damper operating principle is based on the concept that relative motion between adjacent blades takes place during vibration causing relative damper/blade displacements. They dissipate vibratory energy at the damper/blade interfaces by friction and consequently blade resonant amplitudes decrease.

Wedge dampers represent an extremely difficult case because the direct coupling of the two inclined interfaces leads to complex contact kinematics. This aspect was studied in detail by Yang and Menq [6], and Sanliturk, Ewins and Stanbridge [7]. Due to the complexity of the damper behaviour some simplifying assumptions have been made in order to reduce the difficulty of the problem. The main assumption is that damper and platform surfaces remain parallel and in contact at all times, i.e. damper rolling is not permitted.

Damper effect on the dynamical behaviour of the structure is estimated by means of nonlinear forced response calculation of the blade including friction dampers. It can be formulated both in frequency and time domain. However, frequency domain methods are preferable for calculating the steady-state vibration amplitude, instead of the direct time integration, because they are much less time consuming [3].

The Harmonic Balance Method (HBM) is a well-known method to study nonlinear vibration problems in frequency domain. By means of HBM, the system response is supposed to be harmonic, and then the cyclic friction forces are approximated by the first term of their Fourier series [8]. As a result, the set of differential equations obtained by FEM models are transformed in a set of nonlinear algebraic equations in the frequency domain.

Iterative numerical techniques are necessary in order to solve the resulting nonlinear system. The most employed solution technique is the Newton-Raphson Method (NRM). It guarantees quadratic convergence rate when the starting estimate is close to the solution [9].

The most time consuming operation of the NRM is the calculation of the Jacobian matrix, whose terms are the partial derivatives of the nonlinear functions with respect to the unknowns. According to the classical approach, a finite difference scheme is implemented to evaluate the Jacobian of the nonlinear system. Usually, partial derivatives are approximated by discrete incremental ratios. The main problems of this approach are the uncertainty in the choice of the finite increment and the quite long time necessary for the computation of the nonlinear forces in the calculation of the incremental ratio.

A more efficient solving method governing the nonlinear equations is needed. The optimization of the evaluation of Jacobian matrix is crucial for the effective analysis of large systems, specially for the analysis of mistuned assemblies. In [10], large calculation times of the NRM are reduced by means of an analytical approach used to evaluate the Jacobian of the system. The method is proposed for a friction element characterized by Coulomb friction law, 1D relative displacement and variable normal load. By means of the proposed approach, no NRM finite difference scheme is necessary, and large systems can be effectively studied.

As far as we are aware, no study has still been carried out to optimize the calculation procedure of the Jacobian matrix of a system with underplatform wedge dampers, characterized by the kinematic model developed by [6,7].

In this work, the method proposed in [10] is extended to structures with wedge dampers and an exact and complete analytical procedure to be employed in the forced response calculations is developed. It is applied to calculate the frequency response of a real IPT blade under cyclic

symmetry boundary conditions. Excellent results in terms of accuracy and calculation time have been achieved in comparison with numerical NRM.

2. Non-linear forced response calculation

Dynamical equilibrium equation of a structure with friction dampers are

$$\mathbf{M}\cdot\ddot{\mathbf{Q}}(t)+\mathbf{C}\cdot\dot{\mathbf{Q}}(t)+\mathbf{K}\cdot\mathbf{Q}(t)=\mathbf{F_e}(t)-\mathbf{F_d}(\mathbf{Q},t), \tag{1}$$

with

M: mass matrix

C: structural damping matrix

K: stiffness matrix

Q(t): system degrees of freedom (dofs)

$\mathbf{F_e}$(t): external excitation

$\mathbf{F_d}(\mathbf{Q},t)$: contact forces acting on the damper.

They are nonlinear because damper forces depend on displacements of contact points.

Steady-state forced response of the system of Eq. (1) is usually computed by means of the Harmonic Balance Method (HBM) ([1]-[3]). According to HBM, given a harmonic external excitation, the damper forces and the system response are assumed as harmonic with angular frequency equal to that of the excitation. Harmonic coefficients of damper contact forces are evaluated by Fourier expansion of their time histories. Therefore HBM allows to express the forced response of a frictionally damped structure by a set of complex equations in the frequency domain:

$$\overline{\mathbf{Q}}=\overline{\mathbf{Q}}_\mathbf{e}-\overline{\mathbf{R}}\cdot\overline{\mathbf{F}}_\mathbf{d}(\overline{\mathbf{Q}}) \tag{2}$$

where:

$\overline{\mathbf{Q}}$: total response of system dofs.

$\overline{\mathbf{Q}}_\mathbf{e}$: response of system dofs due to external forces.

$\overline{\mathbf{R}}$: receptance matrix.

$\overline{\mathbf{F}}_\mathbf{d}(\overline{\mathbf{Q}})$: First term of Fourier expansion coefficient of $\mathbf{F_d}(\mathbf{Q},t)$

Since contact forces depend only on contact point displacements, vector $\overline{\mathbf{Q}}$ can be divided and only the sub-system

$$\overline{\mathbf{X}}=\overline{\mathbf{X}}_\mathbf{e}-\overline{\mathbf{R}}_\mathbf{d}\cdot\overline{\mathbf{F}}_\mathbf{d}(\overline{\mathbf{X}}) \tag{3}$$

can be computed for contact force evaluation, with

$\overline{\mathbf{X}}$: contact dofs.

$\overline{\mathbf{X}}_\mathbf{e}$: response of contact dofs due to external forces.

$\overline{\mathbf{R}}_\mathbf{d}$: square receptance sub-matrix corresponding to contact dofs

Once contact forces are computed solving equation (3), the forced response of the system can be calculated by means of equation (2).

The subsystem of complex equations (3) may be transformed into the equivalent system of real equations:

$$\mathbf{X} = \mathbf{X_e} - \mathbf{R_d} \cdot \mathbf{F_d}(\mathbf{X}) \tag{4}$$

with:

$$\begin{Bmatrix} X_{(2r-1)} \\ X_{(2r)} \end{Bmatrix} = \begin{Bmatrix} \Re(\overline{X}_{(r)}) \\ \Im(\overline{X}_{(r)}) \end{Bmatrix} \qquad \begin{Bmatrix} X_{e(2r-1)} \\ X_{e(2r)} \end{Bmatrix} = \begin{Bmatrix} \Re(\overline{X}_{e(r)}) \\ \Im(\overline{X}_{e(r)}) \end{Bmatrix} \qquad \begin{Bmatrix} F_{d(2r-1)}(\mathbf{X}) \\ F_{d(2r)}(\mathbf{X}) \end{Bmatrix} = \begin{Bmatrix} \Re\left(\overline{F}_{d(r)}(\overline{\mathbf{X}})\right) \\ \Im\left(\overline{F}_{d(r)}(\overline{\mathbf{X}})\right) \end{Bmatrix}$$

$$\begin{bmatrix} R_{d(2r-1,2s-1)} & R_{d(2r,2s-1)} \\ R_{d(2r-1,2s)} & R_{d(2r,2s)} \end{bmatrix} = \begin{bmatrix} \Re(\overline{R}_{d(r,s)}) & -\Im(\overline{R}_{d(r,s)}) \\ \Im(\overline{R}_{d(r,s)}) & \Re(\overline{R}_{d(r,s)}) \end{bmatrix}$$

Therefore roots of equation (4) are roots of equation (3).

Solution of equation (4) can be computed using Newton-Raphson Method (NRM). It is an iterative procedure that generates a sequence of approximate solutions, converging towards the roots of the system. The approximate solution at the n^{th} step is estimated with the following iterative relationship:

$$\mathbf{X}^{(n)} = \mathbf{X}^{(n-1)} - \mathbf{J}^{(n)^{-1}} \cdot \mathbf{r}(\mathbf{X}^{(n-1)}) \tag{5}$$

where $\mathbf{X}^{(n)}$ is the response vector at the n^{th} iteration, and **r** and **J** are:

$$\mathbf{r}(\mathbf{X}^{(n-1)}) = \mathbf{X}^{(n-1)} - \mathbf{X_e} + \mathbf{R_d} \cdot \mathbf{F_d}(\mathbf{X}^{(n-1)})$$

$$J^{(n)}_{pq} = \frac{\partial r_p(\mathbf{X}^{(n-1)})}{\partial X_q} \quad ,$$

where $\mathbf{J}^{(n)}$ is the Jacobian of the system at the n^{th} iteration and $\mathbf{r}(\mathbf{X}^{(n-1)})$ the residual vector at the $(n-1)^{th}$ iteration. Its terms are the partial derivatives of the nonlinear functions of the system with respect to the unknowns. They can be evaluated numerically by means of a finite difference scheme. The main problem due to such a numerical procedure is that it is time consuming and that calculation time increases remarkably with the number of contact dofs.

In [10], Petrov and Ewins have recently proposed an alternative method which demonstrated excellent performance with respect to speed, accuracy and stability of computation. It is completely analytical and was successfully applied to a single friction element characterised by Coulomb friction law, 1D relative displacement and variable normal load. Namely, Jacobian matrix is evaluated analytically as follows:

$$\mathbf{J}^{(n)} = \frac{\partial \mathbf{r}(\mathbf{X}^{(n-1)})}{\partial \mathbf{X}} = \frac{\partial\left(\mathbf{X} - \mathbf{X_e} + \mathbf{R_d} \cdot \mathbf{F_d}(\mathbf{X})\right)(\mathbf{X}^{(n-1)})}{\partial \mathbf{X}} = \mathbf{I} + \mathbf{R_d} \cdot \frac{\partial \mathbf{F_d}(\mathbf{X}^{(n-1)})}{\partial \mathbf{X}} \tag{6}$$

where **I** is the identity matrix.

In a general case, time history of contact forces is made of several parts. Each part corresponds to a clear-defined damper state. So, Fourier expansion coefficients of the nonlinear contact force can be obtained as a sum of contributions given by each part of the hysteresis cycle. Consider the real part of the first order Fourier expansion coefficients of contact forces:

$$\mathbf{F_C}(\mathbf{X}) = \sum_j \mathbf{F_C}^{(j)}(\mathbf{X}) = \frac{\omega}{\pi} \cdot \sum_j \int_{t_0^{(j)}(\mathbf{X})}^{t_1^{(j)}(\mathbf{X})} \mathbf{F_d}^{(j)}(\mathbf{X},t) \cdot \cos(\omega t)\, dt\,, \tag{7}$$

with

$t_0^{(j)}$: transition time at the beginning of state j.

$t_1^{(j)}$: transition time at the end of state j.

Derivatives of Fourier expansion coefficients of contact forces are:

$$\frac{\partial \mathbf{F_C}(\mathbf{X})}{\partial X_i} = \sum_j \frac{\partial \mathbf{F_C}^{(j)}(\mathbf{X})}{\partial X_i} = \frac{\omega}{\pi} \cdot \sum_j \frac{\partial}{\partial X_i} \left[\int_{t_0^{(j)}(\mathbf{X})}^{t_1^{(j)}(\mathbf{X})} \mathbf{F_d}^{(j)}(\mathbf{X},t) \cdot \cos(\omega t)\, dt \right] \tag{8}$$

Since transition times depend on displacements **X**, equation (8) becomes:

$$\begin{aligned} \frac{\partial \mathbf{F_C}(\mathbf{X})}{\partial X_i} = \frac{\omega}{\pi} \cdot \sum_j \Bigg[& \frac{dt_1^{(j)}(\mathbf{X})}{dX_i} \cdot \mathbf{F_d}^{(j)}(\mathbf{X}, t_1^{(j)}) \cdot \cos(\omega t_1^{(j)}) - \frac{dt_0^{(j)}(\mathbf{X})}{dX_i} \cdot \mathbf{F_d}^{(j)}(\mathbf{X}, t_0^{(j)}) \cdot \cos(\omega t_0^{(j)}) \\ & + \int_{t_0^{(j)}(\mathbf{X})}^{t_1^{(j)}(\mathbf{X})} \frac{\partial \mathbf{F_d}^{(j)}(\mathbf{X},t)}{\partial X_i} \cdot \cos(\omega t)\, dt \Bigg] \end{aligned} \tag{9}$$

Because of periodicity and continuity of contact forces $\mathbf{F_d}(\mathbf{X},t)$ it is

$$\sum_j \left[\frac{dt_1^{(j)}(\mathbf{X})}{dX_i} \cdot \mathbf{F_d}^{(j)}(\mathbf{X}, t_1^{(j)}) \cdot \cos(\omega t_1^{(j)}) - \frac{dt_0^{(j)}(\mathbf{X})}{dX_i} \cdot \mathbf{F_d}^{(j)}(\mathbf{X}, t_0^{(j)}) \cdot \cos(\omega t_0^{(j)}) \right] = 0 \tag{10}$$

In conclusion

$$\frac{\partial \mathbf{F_C}(\mathbf{X})}{\partial X_i} = \frac{\omega}{\pi} \cdot \sum_j \int_{t_0^{(j)}(\mathbf{X})}^{t_1^{(j)}(\mathbf{X})} \frac{\partial \mathbf{F_d}^{(j)}(\mathbf{X},t)}{\partial X_i} \cdot \cos(\omega t)\, dt \tag{11}$$

and, in the same way, for the imaginary part $\mathbf{F_S}(\mathbf{X})$

$$\frac{\partial \mathbf{F_S}(\mathbf{X})}{\partial X_i} = -\frac{\omega}{\pi} \cdot \sum_j \int_{t_0^{(j)}(\mathbf{X})}^{t_1^{(j)}(\mathbf{X})} \frac{\partial \mathbf{F_d}^{(j)}(\mathbf{X},t)}{\partial X_i} \cdot sin(\omega t)\, dt\,. \tag{12}$$

According to equations (11) and (12), analytical formulation of the Jacobian matrix is possible if derivatives of Fourier expansion coefficients of contact forces can be performed analytically.

To the best of our knowledge, a similar study for the case of wedge dampers has not been done yet.

In the next sections, the analytical formulation of equations (11) and (12) will be deduced for a general case of wedge dampers.

Of course, the method described in this section is valid for any damper configuration (blade-to-blade, blade-to ground and underplatform dampers), given a kinematic relationship which links relative displacements to absolute displacements of contact points.

3. Wedge damper model

The wedge damper model adopted here closely follows that developed by [6]. Since the real damper behavior is quite complicated, the model implies some simplifying assumptions:

- damper flexibility and inertia effects are negligible.
- damper and platform surfaces remain in contact at all time.
- damper rolling is not considered.
- damper displacement takes place on the *x*-*y* plane.
- the blade motion is harmonic.

The theoretical formulation of the wedge damper motion is based on the model where relative blade/damper motion is deduced by using absolute motion of both blade platforms.

Underplatform instantaneous motion can be expressed in an *u*-*v* coordinate frame, an oblique coordinate frame defined along the inclined damper surfaces (see Figure 1).

As a consequence of the continuous contact between damper and platforms, they can be used to characterize damper motion as follows:

$$\mathbf{X_d} = \mathbf{U_R} + \mathbf{V_L} \tag{13}$$

$\mathbf{X_d}$: vector of damper displacement.

$\mathbf{U_R}$: vector of absolute displacement of right platform along *u* direction.

$\mathbf{V_L}$: vector of absolute displacement of left platform along *v* direction.

Hence, subscripts 1 and 2 denote left and right damper interface, while L and R denote left and right structure interface, respectively, as showed in Figure 2.

Thus, the relative motions of the blade platforms with respect to the damper can be expressed as:

$$\begin{aligned} u &= (X_L - X_R)\cdot\sin(\alpha) + (Y_L - Y_R)\cdot\cos(\alpha) \\ v &= (X_L - X_R)\cdot\sin(\beta) - (Y_L - Y_R)\cdot\cos(\beta) \end{aligned} \tag{14}$$

with:

u: relative displacement of the left platform with respect to the damper.

v: relative displacement of the right platform with respect to the damper.

X_L and Y_L: horizontal and vertical absolute displacement of left platform blade.

X_R and Y_R: horizontal and vertical absolute displacement of right platform blade.

Tangential loads F_1 and F_2 and normal loads N_1 and N_2 act over both the damper sides, as shown in Figure 1. The induced friction forces are completely characterized by the relative motion between the contact surfaces.

At any time, horizontal and vertical damper equilibrium equations must be satisfied:

$$\begin{aligned} F_1 \sin(\alpha) + N_1 \cos(\alpha) - F_2 \sin(\beta) - N_2 \cos(\beta) = 0 \\ F_1 \cos(\alpha) - N_1 \sin(\alpha) + F_2 \cos(\beta) - N_2 \sin(\beta) + CF = 0 \end{aligned} \tag{15}$$

where CF represents the centrifugal force acting on the damper originated by the disk rotation.

Each interface is modelled with a one-dimensional friction element, as shown in Figure 1b. It consists of a flexible element of stiffness, k_d, and a contact element with friction coefficient μ. This permits to write the expression of the tangential contact force at each damper side valid for any instant as:

$$F_1 = k_d \cdot (u - w_1) \qquad F_2 = k_d \cdot (v - w_2)\,. \tag{16}$$

Friction elements are coupled by damper equilibrium equations. The coupling causes a complex stick-slip mechanism in which the stick-slip motion of the interfaces interact with each other. It results in nine possible coupled damper states: EE, PP, NN, PE, EP, NE, EN, PN and NP. The first character identifies the left contact state whereas the second corresponds to the right contact state. E corresponds to the stick state, P to the positive slip and N to the negative slip of the contact point.

Each state is characterised by a set of equations; in detail:

- State E:

$$F_1 = F_{10} + k_d \cdot u \quad \text{and} \quad \dot{w}_1 = 0 \quad \text{for damper side 1}$$

$$F_2 = F_{20} + k_d \cdot v \quad \text{and} \quad \dot{w}_2 = 0 \quad \text{for damper side 2,}$$

with F_{10} and F_{20} depending on initial conditions of the stick state.

- State P:

$$F_1 = \mu \cdot N_1 \quad \text{and} \quad \dot{w}_1 > 0 \quad \text{for damper side 1}$$

$$F_2 = \mu \cdot N_2 \quad \text{and} \quad \dot{w}_2 > 0 \quad \text{for damper side 2}$$

- State N:

$$F_1 = -\mu \cdot N_1 \quad \text{and} \quad \dot{w}_1 < 0 \quad \text{for damper side 1}$$

$$F_2 = -\mu \cdot N_2 \quad \text{and} \quad \dot{w}_2 < 0 \quad \text{for damper side 2.}$$

Due to coupling of the two damper sides, 32 different transitions can be identified. In general, stick-to-slip transition occurs when the friction force reaches the slipping value; contrarily, slip-to-stick

transition occurs when the contact point inverts its motion. Detailed description of transition criteria can be found in [6].

4. Definition of Jacobian matrix of underplatform dampers

Equation (6) states that in order to define the Jacobian matrix in a complete analytical form, analytical derivatives of Fourier expansion coefficients of the contact forces with respect to the contact absolute displacement must be evaluated.

Once derivatives are obtained, Jacobian matrix can be evaluated through equation (6) and used in equation (5) in the iterative NRM solver.

As previously noted, Jacobian matrix may be expressed as:

$$\mathbf{J}^{(n)} = \mathbf{I} + \mathbf{R_d} \cdot \mathbf{H} \tag{17}$$

with $\mathbf{I}$ identity matrix, $\mathbf{R_d}$ receptance and $\mathbf{H}$ a real 8x8 matrix containing the partial derivatives of the Fourier coefficients of the contact forces with respect to the absolute contact displacements $\mathbf{H} = \frac{\partial \mathbf{F_d}}{\partial \mathbf{X}}\left(\mathbf{X}^{(n-1)}\right)$. Here, $\mathbf{F_d}$ includes real and imaginary part of first order Fourier coefficients of the contact forces and $\mathbf{X}$ includes real and imaginary part of harmonic absolute displacements of contact points, both written in the *x-y* structure coordinate system shown in Figure 2.

The tangential forces over each damper side act along directions *u-v* different from *x-y* and they depend on the relative displacements *u* and *v*. Besides the total contact forces in *x-y* are obtained as linear superposition of both tangential and normal contact forces.

As a consequence, the procedure to obtain the matrix $\mathbf{H}$ is made of four consecutive steps:

1 - Calculate derivatives of Fourier expansion coefficients of tangential contact forces with respect to relative displacements *u* and *v*.

2 - Convert terms obtained at step 1 in derivatives with respect to the absolute displacements $\mathbf{X}$, by means of damper kinematical relationships (14).

3 - Calculate derivatives of Fourier expansion coefficients of normal contact forces by means of damper equilibrium equations (15).

4 - Write terms obtained at step 2 and 3 in structure coordinate system *x-y* by trigonometry relationships.

4.1. Derivatives of Fourier coefficients of tangential forces with respect to u and v.

According to what stated in section 2, in the case of wedge dampers, derivatives of Fourier coefficients of tangential forces with respect to relative displacements are

$$\frac{\partial \mathbf{f_C}(\mathbf{x})}{\partial x_i} = \frac{\omega}{\pi} \cdot \int_0^T \frac{\partial \mathbf{f_d}(\mathbf{x},t)}{\partial x_i} \cdot \cos(\omega t) dt = \sum_j \frac{\partial \mathbf{f_C}^{(j)}(\mathbf{x})}{\partial x_i} = \frac{\omega}{\pi} \cdot \sum_j \int_{t_0^{(j)}(\mathbf{x})}^{t_1^{(j)}(\mathbf{x})} \frac{\partial \mathbf{f_d}^{(j)}(\mathbf{x},t)}{\partial x_i} \cdot \cos(\omega t)\, dt \qquad (18)$$

and

$$\frac{\partial \mathbf{f_S}(\mathbf{x})}{\partial x_i} = -\frac{\omega}{\pi} \cdot \int_0^T \frac{\partial \mathbf{f_d}(\mathbf{x},t)}{\partial x_i} \cdot \sin(\omega t) dt = \sum_j \frac{\partial \mathbf{f_S}^{(j)}(\mathbf{x})}{\partial x_i} = -\frac{\omega}{\pi} \cdot \sum_j \int_{t_0^{(j)}(\mathbf{x})}^{t_1^{(j)}(\mathbf{x})} \frac{\partial \mathbf{f_d}^{(j)}(\mathbf{x},t)}{\partial x_i} \cdot \sin(\omega t)\, dt \qquad (19)$$

with $\mathbf{f_d}(\mathbf{x},t) = \{F_1(\mathbf{x},t), F_2(\mathbf{x},t)\}^T$, $\mathbf{f_C} = \{\Re(\overline{F}_1), \Re(\overline{F}_2)\}^T$, $\mathbf{f_S} = \{\Im(\overline{F}_1), \Im(\overline{F}_2)\}^T$ and $\mathbf{x} = \{\Re(u), \Im(u), \Re(v), \Im(v)\}^T$ and $T = 2\pi/\omega$.

The analytical expression of tangential forces depend on the damper states. In detail:

- **State EE**

$$\begin{aligned} F_1 &= k_d \cdot [u_C \cos(\omega t) - u_S \sin(\omega t)] + F_{10} \\ F_2 &= k_d \cdot [v_C \cos(\omega t) - v_S \sin(\omega t)] + F_{20} \end{aligned}, \qquad (20)$$

- **State PE or NE**

$$\begin{aligned} F_1 &= \frac{\pm\mu}{s \mp \mu \cdot c}(F_2 + CF \cdot cb) \\ F_2 &= k_d \cdot [v_C \cos(\omega t) - v_S \sin(\omega t)] + F_{20} \end{aligned}, \qquad (21)$$

where the upper sign holds for PE and the lower sign to NE.

- **State EP or EN**

$$\begin{aligned} F_1 &= k_d \cdot [u_C \cos(\omega t) - u_S \sin(\omega t)] + F_{10} \\ F_2 &= \frac{\pm\mu}{s \mp \mu \cdot c}(F_1 + CF \cdot ca) \end{aligned}, \qquad (22)$$

where the upper sign holds for EP and the lower sign for EN.

- **State PP, PN, NP or NN**

$$\begin{aligned} F_1 &= \frac{\mu_1\mu_2 ca + \mu_1(s - \mu_2 c)cb}{(s - \mu_1 c)(s - \mu_2 c) - \mu_1\mu_2} CF \\ F_2 &= \frac{\mu_1\mu_2 cb + \mu_2(s - \mu_1 c)ca}{(s - \mu_1 c)(s - \mu_2 c) - \mu_1\mu_2} CF \end{aligned} \qquad (23)$$

with $\mu_1=\mu$ and $\mu_2=\mu$ at PP, $\mu_1=\mu$ and $\mu_2=-\mu$ at PN, $\mu_1=-\mu$ and $\mu_2=\mu$ at NP, $\mu_1=-\mu$ and $\mu_2=-\mu$ at NN, and with $c = \cos(\alpha+\beta)$, $s = \sin(\alpha+\beta)$, $ca=\cos(\alpha)$, $cb=\cos(\beta)$, $sa=\sin(\alpha)$, $sb=\sin(\beta)$. In all the above equations, it is $u_C = \Re(u)$, $u_S = \Im(u)$, $v_C = \Re(v)$, $v_S = \Im(v)$.

As a consequence, the j^{th} term of equations (18) and (19) depends on the damper state, as shown in Table 1, where terms corresponding to the left tangential force F_1 are listed, with

$$I_C = \frac{\omega}{\pi} \int_{t_0^{(j)}(\mathbf{x})}^{t_1^{(j)}(\mathbf{x})} \cos(\omega t)\, dt \quad , \qquad I_S = \frac{\omega}{\pi} \int_{t_0^{(j)}(\mathbf{x})}^{t_1^{(j)}(\mathbf{x})} \sin(\omega t)\, dt \, ,$$

$$I_{CC} = \frac{\omega}{\pi}\int_{t_0^{(j)}(\mathbf{x})}^{t_1^{(j)}(\mathbf{x})} \cos^2(\omega t)\,dt\,, \qquad I_{SS} = \frac{\omega}{\pi}\int_{t_0^{(j)}(\mathbf{x})}^{t_1^{(j)}(\mathbf{x})} \sin^2(\omega t)\,dt\,, \qquad I_{CS} = \frac{\omega}{\pi}\int_{t_0^{(j)}(\mathbf{x})}^{t_1^{(j)}(\mathbf{x})} \cos(\omega t)\cdot\sin(\omega t)\,dt$$

The procedure adopted to obtain the expressions in Table 1 is described for the PE/NE state.

The starting point is Eq. (21)

$$\begin{aligned} \mathrm{F_1} &= \frac{\pm\mu}{\mathrm{s}\mp\mu\cdot\mathrm{c}}\left(\mathrm{F_2} + \mathrm{CF}\cdot\mathrm{cb}\right) \\ \mathrm{F_2} &= \mathrm{k_d}\cdot\left[\mathrm{v_C}\cos(\omega\mathrm{t}) - \mathrm{v_S}\sin(\omega\mathrm{t})\right] + \mathrm{F_{20}} \end{aligned},$$

therefore, if the expression of F_2 is replaced in the first equation, F_1 and F_2 are

$$\begin{aligned} F_1 &= \frac{\pm\mu}{s\mp\mu\cdot c}\left(F_{20} + CF\cdot cb\right) + \frac{\pm\mu}{s\mp\mu\cdot c}\cdot k_d\cdot\left[v_C\cos(\omega t) - v_S\sin(\omega t)\right] \\ F_2 &= k_d\cdot\left[v_C\cos(\omega t) - v_S\sin(\omega t)\right] + F_{20} \end{aligned} \tag{24}$$

Derivatives of the first term of the Fourier series of F_1, as expressed in Eq. (24), with respect to the real and imaginary part of relative displacements *u* and *v* give the relationships listed in Table 1.

Terms corresponding to the right damper force F_2 can be deduced from Table 1 by replacing subscript1 with subscript 2 and switching variables *u* and *v*. In detail terms corresponding to state EE will be in the first column of the resulting table, those corresponding to state PE/NE in the third column, those corresponding to state EP/EN in the second column. Fourth columns does not change at all.

In order to define explicitly the terms listed in Table 1, the derivatives of $F_{10}^{(j)}$ with respect to relative displacements *u* and *v* must be evaluated. The analytical expression of $F_{10}^{(j)}$ and $F_{20}^{(j)}$ depends on the sequence of the damper states.

To obtain the expression of $F_{10}^{(j)}$ and $F_{20}^{(j)}$ for each damper state the following procedure must be applied:

1. write the continuity equations of contact forces $F_1(t)$ and $F_2(t)$ at each transition time, as shown below for the transition between the $(j\text{-}1)^{th}$ and the j^{th} state:

$$\begin{cases} F_1^{(j-1)}(t_1^{j-1}) = F_1^{(j)}(t_0^j) \\ F_2^{(j-1)}(t_1^{j-1}) = F_2^{(j)}(t_0^j) \end{cases} \tag{25}$$

2. Replace both the left and right side terms of equation (25) with the corresponding state equation chosen among equations (20)-(23).
3. Solve the resulting linear system of 2N equations, being N the total number of damper states forming the periodic hysteresis cycle, with $F_{10}^{(j)}$ and $F_{20}^{(j)}$ as unknowns (j = [1:N]).

The analytical evaluation of all possible $F_{10}^{(j)}$ and $F_{20}^{(j)}$ cannot be included in this paper. However, an exhaustive resume can be found in [11].

The sixteen analytical expressions of the derivatives defined at equations (18) and (19) can be assembled in a matrix defined as follows:

$$\left[\frac{\partial \mathbf{f_d}(\mathbf{x})}{\partial \mathbf{x}}\right]=\begin{bmatrix} \frac{\partial F_{1C}}{\partial u_C} & \frac{\partial F_{1C}}{\partial u_S} & \frac{\partial F_{1C}}{\partial v_C} & \frac{\partial F_{1C}}{\partial v_S} \\ \frac{\partial F_{1S}}{\partial u_C} & \frac{\partial F_{1S}}{\partial u_S} & \frac{\partial F_{1S}}{\partial v_C} & \frac{\partial F_{1S}}{\partial v_S} \\ \frac{\partial F_{2C}}{\partial u_C} & \frac{\partial F_{2C}}{\partial u_S} & \frac{\partial F_{2C}}{\partial v_C} & \frac{\partial F_{2C}}{\partial v_S} \\ \frac{\partial F_{2S}}{\partial u_C} & \frac{\partial F_{2S}}{\partial u_S} & \frac{\partial F_{2S}}{\partial v_C} & \frac{\partial F_{2S}}{\partial v_S} \end{bmatrix} \tag{26}$$

4.2. Derivatives of Fourier coefficients of contact forces with respect to X.

In this section, steps 2-4 of the procedure depicted in section 4 are described in details.

At step 2, derivatives contained in matrix $[\partial \mathbf{f_d}(\mathbf{x})/\partial \mathbf{x}]$ of equation (26) must be converted in derivatives with respect to absolute displacements **X**, defined as:

$$\mathbf{X} = \{\Re(X_L), \Im(X_L), \Re(Y_L), \Im(Y_L), \Re(X_R), \Im(X_R), \Re(Y_R), \Im(Y_R)\}^T.$$

Such a conversion can be simply performed by means of damper kinematics equations (14), post-multiplying matrix $[\partial \mathbf{f_d}(\mathbf{x})/\partial \mathbf{x}]$ with a kinematics matrix Λ_K:

$$\left[\frac{\partial \mathbf{f_d}(\mathbf{X})}{\partial \mathbf{X}}\right]=\left[\frac{\partial \mathbf{f_d}(\mathbf{x})}{\partial \mathbf{x}}\right]\cdot[\Lambda_K] \quad [\Lambda_K]=\begin{bmatrix} sa & 0 & ca & 0 & -sa & 0 & -ca & 0 \\ 0 & sa & 0 & ca & 0 & -sa & 0 & -ca \\ sb & 0 & -cb & 0 & -sb & 0 & cb & 0 \\ 0 & sb & 0 & -cb & 0 & -sb & 0 & cb \end{bmatrix}. \tag{27}$$

At step 3, derivatives of Fourier expansion coefficients of normal contact forces must be calculated by means of damper equilibrium equations (15).

At step 4, terms obtained at steps 2 and 3 must be written in structure coordinate system *x-y* by means of trigonometry.

Both operations are performed by pre-multiplying matrix $[\partial \mathbf{f_d}(\mathbf{X})/\partial \mathbf{X}]$ with matrix Λ_F, defined below:

$$[\mathbf{H}]=\left[\frac{\partial \mathbf{F_d}(\mathbf{X})}{\partial \mathbf{X}}\right]=[\Lambda_F]\cdot\left[\frac{\partial \mathbf{f_d}(\mathbf{X})}{\partial \mathbf{X}}\right] \quad [\Lambda_F]=\begin{bmatrix} sa+ca\frac{c}{s} & 0 & \frac{ca}{s} & 0 \\ 0 & -sa-ca\frac{c}{s} & 0 & -\frac{ca}{s} \\ ca-sa\frac{c}{s} & 0 & -\frac{sa}{s} & 0 \\ 0 & -ca+sa\frac{c}{s} & 0 & \frac{sa}{s} \\ -\frac{cb}{s} & 0 & -sb-cb\frac{c}{s} & 0 \\ 0 & \frac{cb}{s} & 0 & sb+cb\frac{c}{s} \\ -\frac{sb}{s} & 0 & cb-sb\frac{c}{s} & 0 \\ 0 & \frac{sb}{s} & 0 & -cb+sb\frac{c}{s} \end{bmatrix}. \quad (28)$$

The matrix **H** obtained at the end of this 4-step procedure can be directly used for the iterative solution of damped systems, such as experimental set-ups usually designed for the characterisation of the underplatform damper.

To solve dynamical systems with underplatform dampers under cyclic symmetry boundary conditions a further step is necessary.

4.3. Wedge damper in cyclic symmetric structure.

As shown in [12-14], the whole dynamic behaviour of a rotationally periodic structure, like blade assemblies, may be deduced from the dynamics of a single periodic sector subject to cyclic symmetry boundary conditions, as shown in Figure 3.

When the single periodic sector of the cyclic symmetric structure includes underplatform dampers, a further transformation of matrix [*H*], defined in the previous section, is necessary in order to express derivatives of Fourier expansion coefficients of contact forces acting on the sector with respect to absolute displacements of the sector contact points.

Applying the technique of complex propagation constant to represent the wave propagation on rotationally periodic structures developed by Thomas [12,13] for linear systems and extended by Petrov [14] to non-linear systems , forces that the k^{th} damper transmits to the structure are related to forces acting on the k^{th} blade by:

$$\begin{aligned} \overline{F}_R &= \overline{F}_1 \\ \overline{F}_L &= \overline{F}_2 \cdot e^{-i\varphi} = \left[\Re(\overline{F}_2)\cos(\varphi)+\Im(\overline{F}_2)sin(\varphi)\right]+i\cdot\left[-\Re(\overline{F}_2)sin(\varphi)+\Im(\overline{F}_2)\cos(\varphi)\right] \end{aligned} \quad (29)$$

with φ the interblade phase angle, defined by:

$$\varphi = 2\pi \cdot \frac{EO}{N_B}$$

and with N_B the number of turbine blades and EO the engine order.

Similar relationships link the absolute displacements of the nodes of the structure in contact with the k^{th} damper to the absolute displacements of the contact points of the k^{th} blade.

$$\begin{aligned} \overline{X}_1 &= \overline{X}_R \\ \overline{X}_2 &= \overline{X}_L \cdot e^{i\varphi} = \left[\Re(\overline{X}_L)\cos(\varphi) - \Im(\overline{X}_L)sin(\varphi)\right] + i \cdot \left[\Re(\overline{X}_L)sin(\varphi) + \Im(\overline{X}_L)\cos(\varphi)\right] \end{aligned} \quad (30)$$

Relationships expressed by equations (29) and (30) can be resumed in a cyclic symmetric transformation matrix Λ_{SC}. Finally, matrix $[H]_{SC}$ for the fundamental sector under cyclic symmetry is obtained doing:

$$[\mathbf{H}]_{SC} = [\Lambda_{SC}]^T \cdot [\mathbf{H}] \cdot [\Lambda_{SC}] \text{ with } [\Lambda_{SC}] = \begin{bmatrix} \cos(\varphi) & -\sin(\varphi) & 0 & 0 & 0 & 0 & 0 & 0 \\ \sin(\varphi) & \cos(\varphi) & 0 & 0 & 0 & 0 & 0 & 0 \\ 0 & 0 & \cos(\varphi) & -\sin(\varphi) & 0 & 0 & 0 & 0 \\ 0 & 0 & \sin(\varphi) & \cos(\varphi) & 0 & 0 & 0 & 0 \\ 0 & 0 & 0 & 0 & 1 & 0 & 0 & 0 \\ 0 & 0 & 0 & 0 & 0 & 1 & 0 & 0 \\ 0 & 0 & 0 & 0 & 0 & 0 & 1 & 0 \\ 0 & 0 & 0 & 0 & 0 & 0 & 0 & 1 \end{bmatrix} \quad (31)$$

5. Application to a real IPT blade

The proposed method is applied to the forced response calculation of a real intermediate pressure turbine (IPT) blade under cyclic symmetry boundary conditions subjected to 66th engine order excitation which affects the blade's third bending mode (3F). The number of blades is 100. Structural model is obtained via standard finite element formulation in a commercial FEM software. The Component Mode Synthesis CMS (Craig-Bampton, [15]) condensation was used, keeping contact nodes and the first fourteen modal coordinates.

Damper geometry corresponds to the family of underplatform wedge dampers having flat faces with base angles α and β equal to 60° and 30°, respectively. The parameters of the system and the friction interface are all given in consistent system of units.

The number of contact points along the damper sides is progressively increased from 1 up to 4, in order to test the efficiency of the proposed Analytical Method (AM) and to compare it to the classical Newton Raphson Method (NRM), based on a finite difference scheme. A wide range of damper masses is studied.

In order to select the N contact points over each blade platform the following procedure is adopted (Figure 4):

1. the contact area is divided into N equally spaced sectors disposed along the longitudinal axis of the system (axis z).
2. For each sector, the contact point is taken in the middle of the sector.

In Figure 5 the amplitude corresponding to the blade 3rd bending mode is plotted against the excitation angular frequency for 4-contact-point configuration. The abscissa axis is normalised to the resonance angular frequency ω_n of the linear blade without friction dampers. Left and right peaks correspond to the linear cases, whilst other curves represent responses for intermediate values of damper mass (centrifugal force). Damper mass is normalised to the optimal value.

Results for blade response are equivalent for both methods; it confirms the correctness of the analytical expressions used to compute the Jacobian matrix of the system and implemented in the numerical code. According to the solving method used, different number of iterations are performed to achieve the required tolerance. In Figure 6 a representative example of the number of iterations required to calculate the solution for the optimal damper mass is shown for both methods. The analytical method proved to be more stable and to find equation roots with fewer iteration than numerical NRM.

The excellent efficiency obtained by the analytical method is due not only to the lesser number of iterations but also the higher speed at which they are computed. In Table 2 calculation times for 4 contact point configuration obtained with proposed AM and those for classical NRM are listed. They are normalized with total calculation time spent by the classical NRM.

Proposed method showed to be more efficient than the NRM for any number of contact points. In detail, its benefit becomes higher as the number of contact points increases, as shown in Figure 7, where total elapsed time spent on the calculation of FRFs versus number of contact points is represented for both methods. Calculation times are normalized in order to have the unit value in case of 1 contact point computed with the numerical NRM.

Calculation time for the analytical method grows linearly with the number of contact points with a slope much smaller than that of the numerical NRM.

The linear growth of calculation times with respect to the number of contact points observed in Figure 7 cannot be a priori extended also to systems characterized by a larger number of contact points.

In detail, at the generic n^{th} iteration, the following quantities are computed, given a starting vector $\mathbf{X}^{(n-1)}$:

1. the vector of Fourier coefficients of contact forces $\mathbf{F_d(X^{(n-1)})}$

2. the matrix $\frac{\partial \mathbf{F_d}\left(\mathbf{X}^{(n-1)}\right)}{\partial \mathbf{X}}$ containing derivatives of Fourier coefficients of contact forces $\mathbf{F_d(X^{(n-1)})}$ with respect to **X.**
3. the vector of residuals $\mathbf{r}\left(\mathbf{X}^{(n-1)}\right)$
4. the Jacobian matrix $\mathbf{J}^{(n)}$
5. the vector $\mathbf{X}^{(n)} = \mathbf{X}^{(n-1)} - \mathbf{J}^{(n)^{-1}} \cdot \mathbf{r}(\mathbf{X}^{(n-1)})$.

The number of operations necessary to perform step 1 and step 2 grows linearly with the number of contact DOFs.

In steps 3, 4 and 5, the most time consuming operation is the computation of term $\mathbf{X}^{(n)}$ because it needs the solution of the linear system $\mathbf{J}^{(n)^{-1}} \cdot \mathbf{r}\left(\mathbf{X}^{(n-1)}\right)$. For example if direct methods such as the Cholesky factorization are employed, the number of operations increases proportionally to the cube of the number of contact DOFs.

In conclusion, since the methodology described in this paper only affects step 2, time savings per iteration due to its implementation increase linearly with the number of contact DOFs, but total calculation time in case of a very large number of contact DOFs may manifest a non-linear growth with respect to the number of contact DOFs.

6. Conclusions

In this paper an analytical method for the forced response calculation of dynamical systems having wedge dampers by means of iterative Newton-Raphson scheme has been formulated. The method allows to evaluate analytically the Jacobian matrix of the system at each step. It is exact, completely analytical and optimizes the calculation of derivatives of nonlinear contact force Fourier expansion coefficients with respect to structure absolute displacements.

The proposed method is inspired to the method developed by Petrov and Ewins ([10]) for a particular friction damper configuration and has been extended to a wedge damper model. It is applicable to any type of structures, including those characterized by cyclic symmetry boundary conditions.

The numerical code POLI-Damper in which the procedure has been included, can be integrated with some of the most popular standard finite element codes.

The method has been successfully applied to compute the forced response of a real intermediate pressure turbine blade under cyclic symmetry boundary conditions with underplatform wedge dampers.

It has been compared to the classical numerical Newton-Raphson Method based on finite different scheme within a large range of damper masses. Comparison shows that the proposed method allows up to about 80% of time savings with respect to the classical Newton-Raphson scheme without loss of precision.

The total amount of time savings grows as the number of contact points increases. As a consequence, it looks promising for being employed also in forced response calculation of mistuned blade assemblies with wedge dampers, where cyclic symmetry boundary conditions cannot be applied and the whole assembly must be analyzed.

References

1. Griffin J.H., Friction Damping of Resonant Stresses in Gas Turbines Airfoils, *ASME Journal of Engineering for power*, **102**, 329 (1980).
2. Cameron T.M., Griffin J.H., Kielb R.E., Hoosac T.M., An Integrated Approach for Friction Damper Design, *ASME Journal of Vibration, Acoustics, Stress and Reliability in Design*, **112**, 175 (1990).
3. Sanliturk K.Y., Imregun M., Ewins D.J., Harmonic Balance Vibration Analysis of Turbine Blades with Friction Dampers, *ASME Journal Vibration and Acoustics*, **119**, 96 (1997).
4. Srinivasan A.V., Flutter and Resonant Vibration Characteristics of Engine Blades, *Journal of Engineering for Gas Turbines and Power, Transactions of the ASME*, **119**, 742 (1997).
5. Griffin J.H., A Review of Friction Damping of Turbine Blade Vibration, *International Journal of Turbo and Jet Engines*, **7**, 297 (1990).
6. Yanq B.D., Menq C.H., Characterization of Contact Kinematics and Application to the Design of Wedge Damper in Turbomachinery Blading: Part 1-Stick-Slip Contact Kinematics, *ASME Journal of Engineering for Gas Turbines and Power*, **120**, 410 (1998).
7. Sanliturk K.Y., Ewins D.J., Stanbridge A.B., Underplatform Damper for Turbine Blades: Theoretical Modelling, Analysis and Comparison with Experimental Data, *ASME Journal of Engineering for Gas Turbines and Power*, **123**, 919 (2001).
8. Menq C.H., *The Vibratory Response of Frictionally Constrained Gas Turbine Engine Blades* PhD Dissertation, Carnegie-Mellon University, Pittsburgh (1985).
9. Dennis J.E., Schnabel R.B. *Numerical Methods for Unconstrained Optimisation and Non-linear Equations*, Prentice-Hall, Englewood Cliffs (1983).
10. Petrov E.P., Ewins D.J., Analytical Formulation of Friction Interface Elements for Analysis of Nonlinear Multi-Harmonic Vibrations of Blade Discs, *ASME Journal of Turbomachinery*, **125**, 364 (2003).

11. Borrajo J.M., *Dynamics of Cyclic Symmetric Structures having Nonlinear Friction Damping*, PhD Dissertation, Politecnico di Torino, Torino (2005).
12. Thomas D.L., Standing Waves in Rotationally Periodic Structures, *Journal of Sound and Vibration*, **37**, 288 (1974).
13. Thomas D.L., Dynamic of Rotationally Periodic Structures, *International Journal for Numerical Methods in Engineering*, **37**, 81 (1979).
14. Petrov E.P., A Method for Use of Cyclic Symmetry Properties in Analysis of Nonlinear Multiharmonic Vibrations of Bladed Discs, *ASME Journal of Turbomachinery*, **126**, 175 (2004).
15. Craig R.R., Bampton M.C., Coupling of structures for dynamic analyses, *AIAA Journal*, **6**, 1313 (1968).

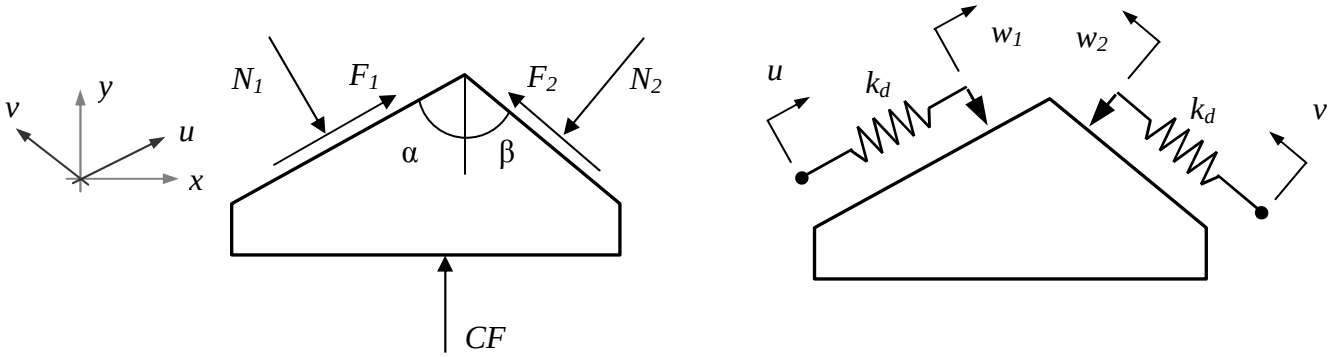

Figure 1. Forces acting on a damper, and model of a wedge damper.

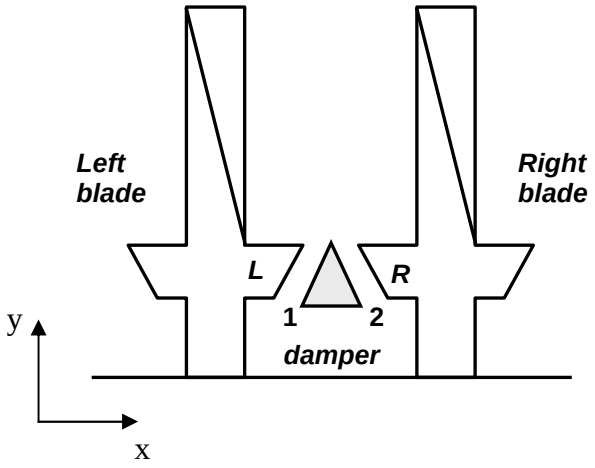

Figure 2. Damper and bladed structure.

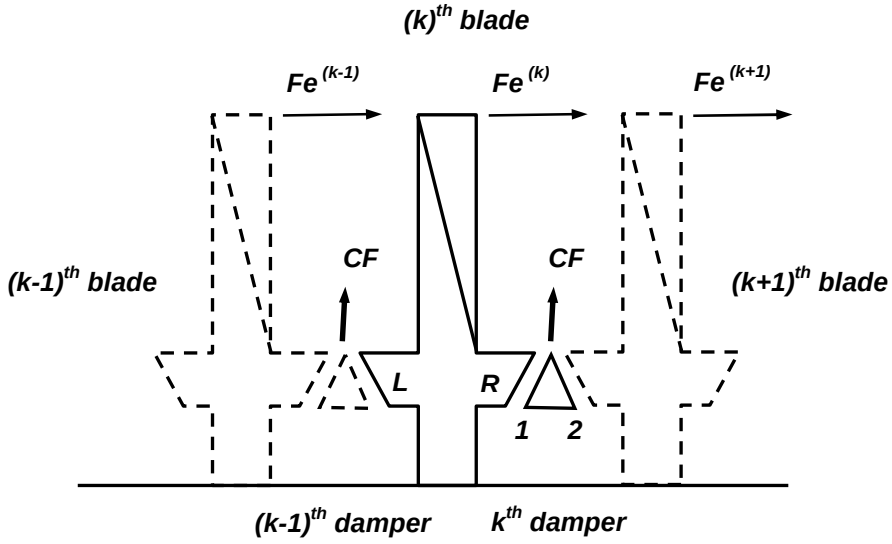

Figure 3. Scheme of a cyclic symmetric blade assembly. The fundamental sector, made of one blade and one damper, is drawn in continuous line.

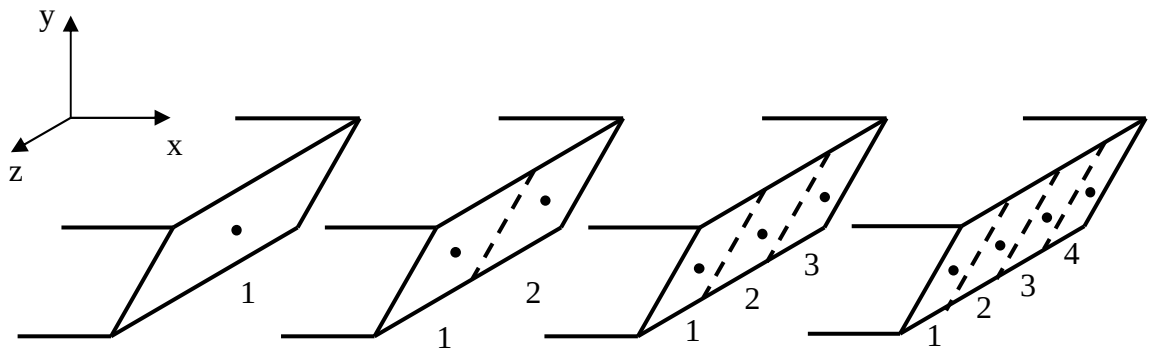

Figure 4. Contact point selection on blade platform

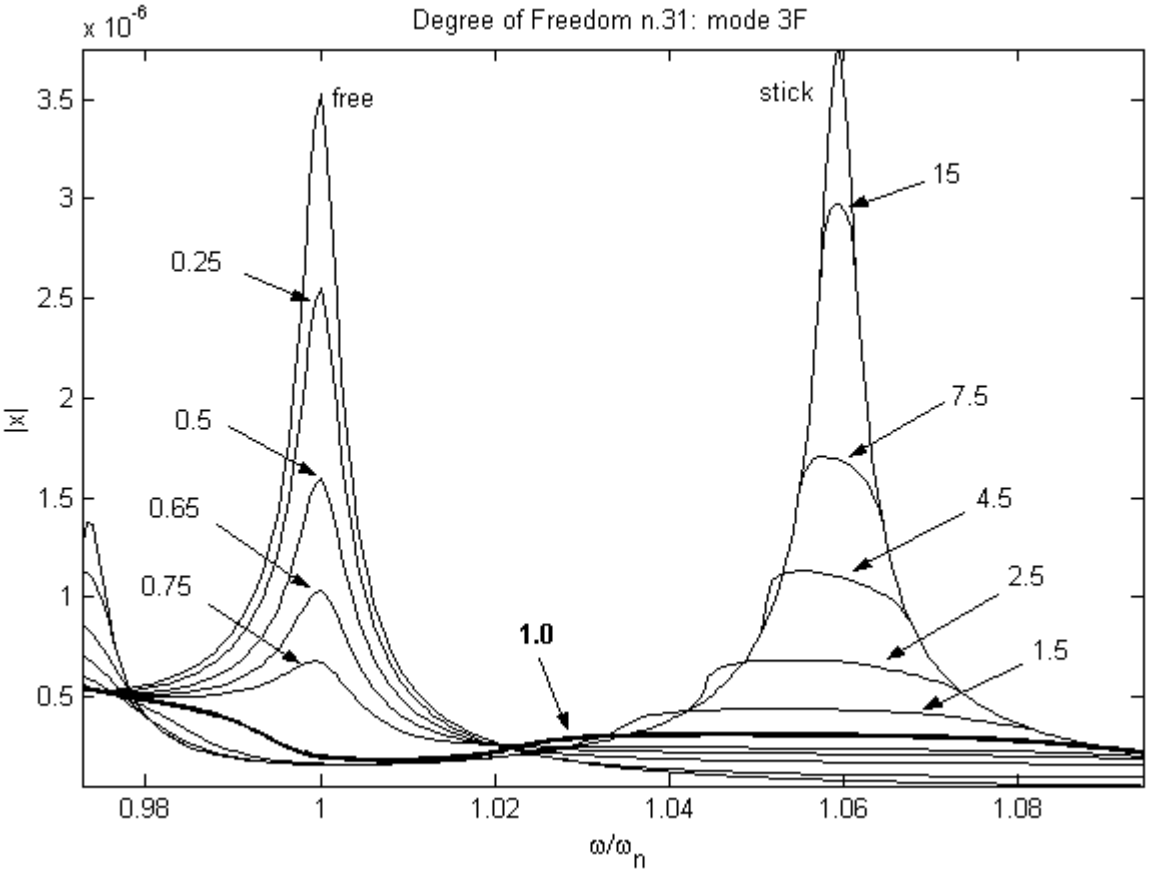

Figure 5. FRF of 3rd bending mode for 4-contact-point configuration.

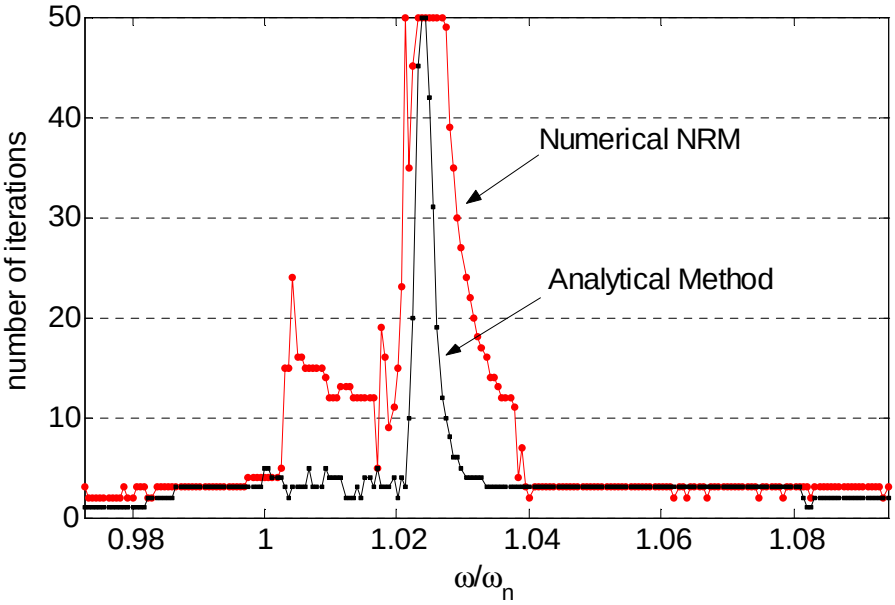

Figure 6. Number of iterations required to calculate the FRF corresponding to the optimal damper mass for both methods.

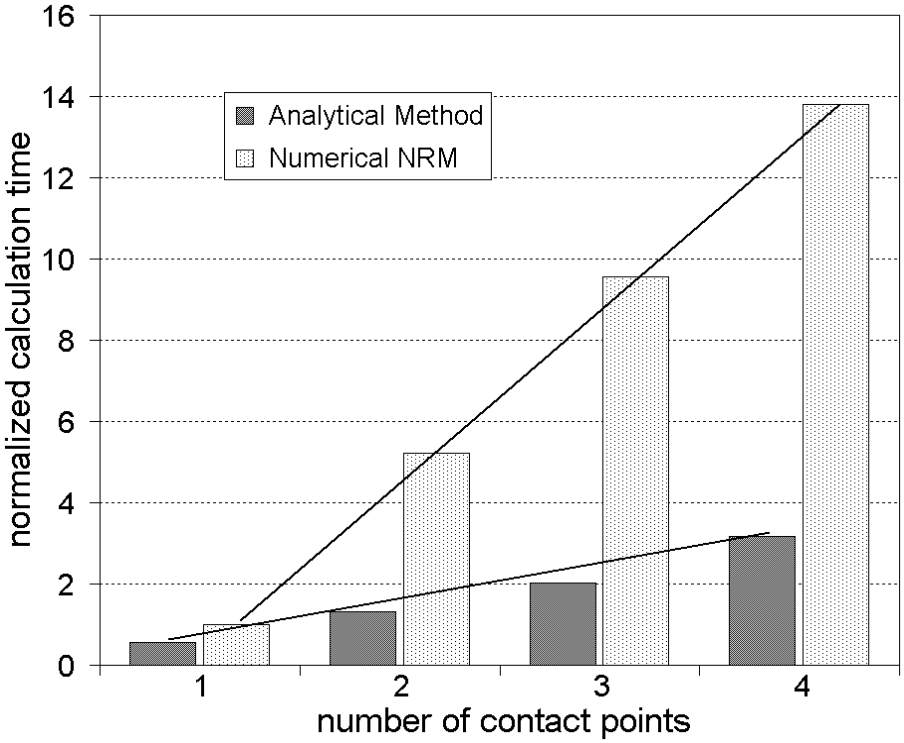

Figure 7. Normalized calculation times against number of contact points for the classical Newton-Raphson method and the analytical method.

Table 1

Table 1. Expressions for the derivatives of Fourier coefficients of tangential forces on the left damper interface with respect to relative displacements.

State	**EE**	**PE/NE**	**EP/EN**	**PP, PN, NP, NN**
$\frac{\partial F_{1C}^{(j)}}{\partial u_C}$	$\frac{\partial F_{10}^{(j)}}{\partial u_C} \cdot I_C + k_d \cdot I_{CC}$	$\frac{\pm\mu}{s \mp \mu \cdot c} \cdot \frac{\partial F_{20}^{(j)}}{\partial u_C} \cdot I_C$	$\frac{\partial F_{10}^{(j)}}{\partial u_C} \cdot I_C + k_d \cdot I_{CC}$	0
$\frac{\partial F_{1C}^{(j)}}{\partial u_S}$	$\frac{\partial F_{10}^{(j)}}{\partial u_S} \cdot I_C - k_d \cdot I_{CS}$	$\frac{\pm\mu}{s \mp \mu \cdot c} \cdot \frac{\partial F_{20}^{(j)}}{\partial u_S} \cdot I_C$	$\frac{\partial F_{10}^{(j)}}{\partial u_S} \cdot I_C - k_d \cdot I_{CS}$	0
$\frac{\partial F_{1C}^{(j)}}{\partial v_C}$	$\frac{\partial F_{10}^{(j)}}{\partial v_C} \cdot I_C$	$\frac{\pm\mu}{s \mp \mu \cdot c}\left[\frac{\partial F_{20}^{(j)}}{\partial v_C} \cdot I_C + k_d \cdot I_{CC}\right]$	$\frac{\partial F_{10}^{(j)}}{\partial v_C} \cdot I_C$	0
$\frac{\partial F_{1C}^{(j)}}{\partial v_S}$	$\frac{\partial F_{10}^{(j)}}{\partial v_S} \cdot I_C$	$\frac{\pm\mu}{s \mp \mu \cdot c}\left[\frac{\partial F_{20}^{(j)}}{\partial v_S} \cdot I_C - k_d \cdot I_{CS}\right]$	$\frac{\partial F_{10}^{(j)}}{\partial v_S} \cdot I_C$	0
$\frac{\partial F_{1S}^{(j)}}{\partial u_C}$	$-\frac{\partial F_{10}^{(j)}}{\partial u_C} \cdot I_S - k_d \cdot I_{CS}$	$\frac{\mp\mu}{s \mp \mu \cdot c} \cdot \frac{\partial F_{20}^{(j)}}{\partial u_C} \cdot I_S$	$-\frac{\partial F_{10}^{(j)}}{\partial u_C} \cdot I_S - k_d \cdot I_{CS}$	0
$\frac{\partial F_{1S}^{(j)}}{\partial u_S}$	$-\frac{\partial F_{10}^{(j)}}{\partial u_S} \cdot I_S + k_d \cdot I_{SS}$	$\frac{\mp\mu}{s \mp \mu \cdot c} \cdot \frac{\partial F_{20}^{(j)}}{\partial u_S} \cdot I_S$	$-\frac{\partial F_{10}^{(j)}}{\partial u_S} \cdot I_S + k_d \cdot I_{SS}$	0
$\frac{\partial F_{1S}^{(j)}}{\partial v_C}$	$-\frac{\partial F_{10}^{(j)}}{\partial v_C} \cdot I_S$	$\frac{\mp\mu}{s \mp \mu \cdot c}\left[\frac{\partial F_{20}^{(j)}}{\partial v_C} \cdot I_S + k_d \cdot I_{CS}\right]$	$-\frac{\partial F_{10}^{(j)}}{\partial v_C} \cdot I_S$	0
$\frac{\partial F_{1S}^{(j)}}{\partial v_S}$	$-\frac{\partial F_{10}^{(j)}}{\partial v_S} \cdot I_S$	$\frac{\mp\mu}{s \mp \mu \cdot c}\left[\frac{\partial F_{20}^{(j)}}{\partial v_S} \cdot I_S - k_d \cdot I_{SS}\right]$	$-\frac{\partial F_{10}^{(j)}}{\partial v_S} \cdot I_S$	0

Table 2. Normalized calculation times for 4-contact-point configuration.

Normalized damper mass	0.25	0.5	0.65	0.75	1	1.5	2.5	4.5	7.5	**TOT**
NRM	3,8%	3,9%	4,4%	4,8%	21,7%	21,5%	22,1%	15,7%	2,2%	**100%**
AM	0,5%	0,5%	0,6%	1,0%	5,7%	5,4%	5,0%	3,2%	1,0%	**23%**